Protein Science (2000), *9*:1120–1128. Cambridge University Press. Printed in the USA.

Tumor suppressor INK4: Refinement of $p16^{INK4A}$ structure and determination of $p15^{INK4B}$ structure by comparative modeling and NMR data

CHUNHUA YUAN,[1,5] THOMAS L. SELBY,[1,5] JUNAN LI,[2] IN-JA L. BYEON,[3] AND MING-DAW TSAI[1,2,3,4]

[1]Department of Chemistry, The Ohio State University, Columbus, Ohio 43210
[2]Department of Biochemistry, The Ohio State University, Columbus, Ohio 43210
[3]Campus Chemical Instrument Center, The Ohio State University, Columbus, Ohio 43210
[4]Ohio State Biochemistry Program, The Ohio State University, Columbus, Ohio 43210

(RECEIVED November 24, 1999; FINAL REVISION March 29, 2000; ACCEPTED April 9, 2000)

Abstract

Within the tumor suppressor protein INK4 (inhibitor of cyclin-dependent kinase 4) family, $p15^{INK4B}$ is the smallest and the only one whose structure has not been determined previously, probably due to the protein's conformational flexibility and instability. In this work, multidimensional NMR studies were performed on this protein. The first tertiary structure was built by comparative modeling with $p16^{INK4A}$ as the template, followed by restrained energy minimization with NMR constraints (NOE and H-bonds). For this purpose, the solution structure of $p16^{INK4A}$, whose quality was also limited by similar problems, was refined with additional NMR experiments conducted on an 800 MHz spectrometer and by structure-based iterative NOE assignments. The nonhelical regions showed major improvement with root-mean-square deviation (RMSD) improved from 1.23 to 0.68 Å for backbone heavy atoms. The completion of $p15^{INK4B}$ coupled with refinement of $p16^{INK4A}$ made it possible to compare the structures of the four INK4 members in depth, and to compare the structures of $p16^{INK4A}$ in the free form and in the $p16^{INK4A}$-CDK6 complex. This is an important step toward a comprehensive understanding of the precise functional roles of each INK4 member.

Keywords: comparative modeling; NMR spectroscopy; $p15^{INK4B}$; $p16^{INK4A}$; protein structure

The INK4 family of ankyrin-repeat proteins consists of four members that range in size from 13.7–18 kDa: $p15^{INK4B}$ (Hannon & Beach, 1994), $p16^{INK4A}$ (Serrano et al., 1993), $p18^{INK4C}$ (Guan et al., 1994), and $p19^{INK4D}$ (Guan et al., 1996) (abbreviated hereafter as p15, p16, p18, and p19, respectively). They show more than 40% sequence homology, and all have been verified to bind to CDK4 and CDK6 *in vivo* and inhibit the kinase activity *in vitro*. The inhibition is known to occur during the cell cycle at the G1/S transition when INK4 binding inhibits the kinase function of promoting cell cycle progression via the phosphorylation of the retinoblastoma gene product (pRB) (Sherr, 1996).

Of the genes in the INK4 family, by far the greatest number of alterations has been discovered in that of p16. These include promoter methylation (Pinyol et al., 1998), genetic deletions (Tsutsumi et al., 1998), and missense mutations (MacKie et al., 1998). The smallest member, p15, has also been reported to have promoter methylation (Malumbres et al., 1997) and deletions (Glendening et al., 1995), which occur independently of or concurrently with p16 alterations (Hamada et al., 1998). On the other hand, the two larger family members, p18 and p19, have shown very few genetic alterations in cancer cell lines (Gemma et al., 1996). Indeed, in some cases hepatoblastoma alterations of p16 and p15 have occurred in the absence of any such alterations in p18, demonstrating that INK4 family members cannot substitute for one another following a genetic alteration (Iolascon et al., 1996). Differential expression of the INK4 family members has also been studied in the mouse model (Zindy et al., 1997), in which p18 and

Reprint requests to: M.-D. Tsai, Department of Chemistry, The Ohio State University, 100 West 18th Avenue, Columbus, Ohio 43210-1185; e-mail: Tsai@chemistry.ohio-state.edu.

[5]These two authors contributed equally to this paper.

Abbreviations: 2D, 3D, 4D, two-, three-, and four-dimensional; CDK, cyclin-dependent kinase; DTT, dithiothreitol; EDTA, ethylenediaminetetraacetic acid; GST, glutathione S-transferase; H-T-H, helix-turn-helix; HEPES, *N*-(2-hydroxyethyl)-piperazine-*N′*-(2-ethanesulfonic acid); HMQC, heteronuclear multiple quantum coherence; HSQC, heteronuclear single-quantum coherence; INK4, inhibitor of CDK4; NOE, nuclear Overhauser enhancement; NOESY, nuclear Overhauser enhancement correlated spectroscopy; p15, CDK inhibitor $p15^{INK4B}$; p16, CDK inhibitor $p16^{INK4A}$; p18, CDK inhibitor $p18^{INK4C}$; p19, CDK inhibitor $p19^{INK4D}$; RMSD, root-mean-square deviation; TOCSY, total correlation spectroscopy.

p19 were widely expressed during embryogenesis whereas p15 and p16 were not detected. Furthermore, p16 and p18 levels increased as the cells approached senescence. Reports such as these strongly support the suggestion that the four INK4 proteins are not physiologically redundant (Sherr, 1996), and thus stress the need for detailed study of each member.

Despite the short history of INK4 studies, the protein structures have been examined extensively by X-ray and NMR due to the significance in cancer research. In less than a 2 yr span, the following structures have been reported: the solution structure of mouse p19 (Luh et al., 1997), crystal structure of human p18 (Venkataramani et al., 1998), solution structure of human p16 (Byeon et al., 1998), crystal structure of human p19 (Baumgartner et al., 1998), and solution structure of human p18 (Li et al., 1999). The results showed that they all adopt a similar overall fold, which includes an array of four (p16) or five (p18 and p19) helix-turn-helix (H-T-H) motifs connected by long loops. More importantly, the crystal structures of the p16-CDK6 (Russo et al., 1998) and p19-CDK6 complexes (Brotherton et al., 1998; Russo et al., 1998) have been determined, providing unprecedented insights into the CDK binding of INK4 proteins.

Due to the structural flexibility and instability probably inherent in the smaller INK4 members (Yuan et al., 1999), the NMR-derived p16 structure was determined at relatively low resolution, while the p15 structure is not yet available. No crystal structure has been reported for either protein in the free form. In this paper we present the NMR results for mouse p15. Assisted by comparative modeling with human p16 as the template, the first tertiary structure of p15 was built with a limited number (672 in total) of NMR constraints. For this purpose, we also refined the p16 solution structure by repeating NMR experiments on an 800 MHz spectrometer and by structure-based iterative NOE assignments (Nilges, 1996). Knowledge of the p15 structure coupled with the refinement of p16 has allowed us to compare the structures of different INK4 proteins in detail. This is an important step toward understanding the properties of each INK4 member, such as differing specificity and affinity for CDK, that relate to their potentially different cellular functions.

Results

Refinement of the p16 structure

The solution structure of free p16 was reported in two stages—total assignment and secondary structure in 1996 (Tevelev et al., 1996), and tertiary structure in 1998 (Byeon et al., 1998). The latter was elucidated at only a modest resolution according to current standards. In this work, 260 additional NOEs including 40 long range ones ($i - j > 5$) were added to the initial 1,437. The p16 structure generated with these constraints as well as with dihedral angle and $^{13}C^{\alpha}/^{13}C^{\beta}$ chemical shift restraints showed a substantial improvement in terms of RMSD (Table 1). The nonhelical regions in particular are much better defined, with an RMSD improved from 1.23 to 0.68 Å for backbone heavy atoms (Fig. 1). Some critical NOEs, identified in the loops, are suggestive of three short β-sheets involving the following residues: 41–42, 46–47 (β1), 73–74, 79–80 (β2), 107–108, and 112–113 (β3) (Fig. 2). The β1 turn and β2 turn may interact loosely as indicated by only two weak NOEs assigned to $H^{\alpha 1}(45)/H^{\alpha}(74)$ and $H^{\alpha 2}(45)/H^{\alpha}(74)$, while the β2 turn and β3 turn seem to interact more intimately as evidenced by many side-chain contacts. These three short β-sheets do not appear to form a continuous β-sheet, as the crucial evidence such as $H^{\alpha}(79)/H^{\alpha}(108)$ was not observed. Overall, the improvements allowed for p16 to better serve as a template for determination of the p15 structure, and for a more detailed comparison between p16 and other INK4 proteins.

Assignments in p15 were aided by p16 results

The p15 protein presents the same structural problems (low stability and high flexibility) as p16 but to an even greater extent (Yuan et al., 1999). For instance, amide protons were almost com-

Table 1. *Structural statistics for the refined p16 structures*[a]

	⟨SA⟩	Previous ⟨SA⟩
RMSD from experimental constraints (Å)		
NOE distances (Å) (1,695)	0.021 ± 0.001	0.018 ± 0.001
Dihedral angles (°) (63)	0.07 ± 0.03	0.12 ± 0.05
$^{13}C^{\alpha}$ constraints (ppm) (69)	0.90 ± 0.05	
$^{13}C^{\beta}$ constraints (ppm) (58)	0.78 ± 0.04	
RMSD from idealized covalent geometry		
Bonds (Å)	0.0026 ± 0.0002	0.0011 ± 0.0001
Angles (°)	0.58 ± 0.01	0.54 ± 0.01
Impropers (°)	0.39 ± 0.01	0.35 ± 0.002
Atomic RMSD between ⟨SA⟩ and SA		
Backbone heavy atoms for residues 14–134	0.57 ± 0.05	0.95 ± 0.10
All heavy atoms for residues 14–134	1.08 ± 0.08	1.45 ± 0.13
Backbone heavy atoms for helical residues[b]	0.43 ± 0.05	0.58 ± 0.10
All heavy atoms for helical residues[b]	0.88 ± 0.06	1.06 ± 0.09

[a] ⟨SA⟩ represents the average RMSD for the ensemble. The number of various restraints is given in parentheses. None of the ⟨SA⟩ structures exhibited distance violations >0.5 Å or dihedral angle violations >5°. For comparisons the previous ⟨SA⟩ values were listed in the last column (Byeon et al., 1998).

[b] Residues 15–21, 25–33, 48–51, 57–65, 81–87, 91–99, 114–120, and 124–133 are identified as helical residues.

Fig. 1. Stereoview showing the best-fit superposition of the backbone (N, C^{α}, C) atoms of the 19 refined p16 structures. The random segments at the N-terminus (residues 1–13) and the C-terminus (residues 135–156) are not shown.

pletely exchanged after only a few minutes in D_2O at 20 °C (Fig. 3), which is a clear indication of great structural flexibility. A typical sample at 250 μM lasted only three or four days before it denatured and aggregated. As a result, 3D NMR spectra have a low signal-to-noise ratio. For example, in the 3D HCCH-TOCSY experiment, only the residues in random coil showed strong peaks. However, mouse p15 shows more than 86% sequence homology to human p16. Aided by the p16 results, all but five (S5, R37, T71, L72, and A103) backbone amides of p15 have been assigned or tentatively assigned (R97 and D102) with triple resonance experiments and 3D ^{15}N-NOESY-HSQC (Fig. 4). In addition, about 94% of H^{α}, 88% of H^{β}, and roughly 70% of all other side-chain protons have been assigned. p15, as expected, displays a chemical shift dispersion similar to that of p16. Figure 5 shows the combined ^{1}H and ^{15}N chemical shift differences for the backbone amides of the two proteins in alignment. The average values are just 0.16 ± 0.12 and 0.35 ± 0.23 ppm for identical and nonidentical residues, respectively, in the region of 10–127 (excluding R97). The major differences were found in loops and turns, for example, loop 1 (N33, A34, and N36 in p15) and turn 3 (E82 and G83 in p15), which may implicate relatively large structural differences between p15 and p16 in these regions.

p15 assumes a similar secondary structure as well as tertiary fold to p16

Like other INK4 proteins, p15 was shown to possess a largely α-helical conformation on the basis of circular dichroism experiments (data not shown). NMR data coupled with the structural analysis in other members suggests that the segments of 8–16, 19–28, 51–60, 76–82, 85–94, 109–115, and 118–127 are in a helical conformation, though the exact length of each helix could be varied by one or two residues. The experimental evidence can be summarized as follows. First, almost all $^{13}C^{\alpha}$ carbons predicted to be in a helical conformation experience a downfield shift from the respective random coil values (Fig. 6A) (Spera & Bax, 1991). Second, the short-range NOEs, particularly 29 $H^{\alpha}(i)/H^{\beta}(i+3)$ NOEs shown in Figure 6B, are characteristic of the α-helical conformation (Wüthrich, 1986). Third, we have previously deter-

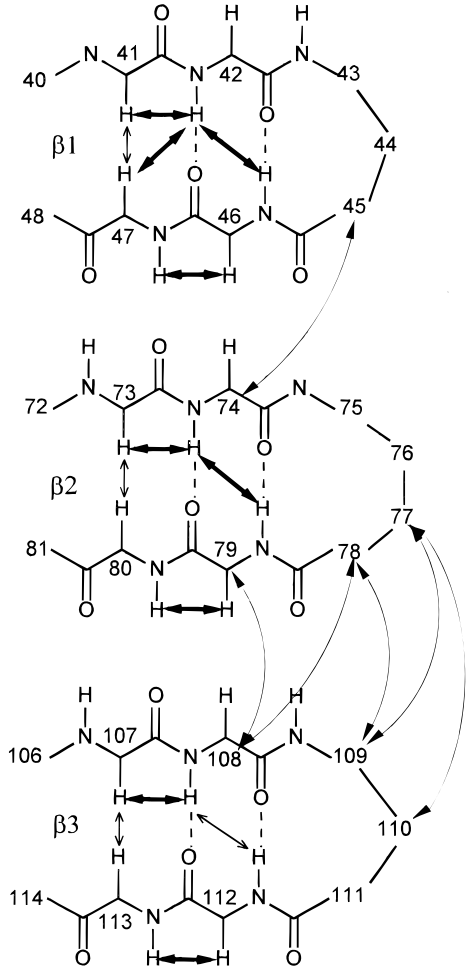

Fig. 2. Proposed β-sheets in p16 from NMR data. The thick arrows indicate medium or strong NOEs, while the thin arrows refer to weak or very weak NOEs. The curved arrows mark the side chain interactions observed in NMR spectroscopy.

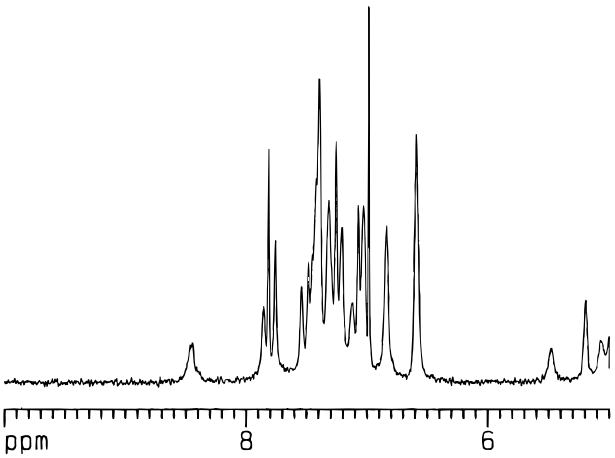

Fig. 3. One-dimensional proton NMR spectrum of p15 recorded immediately following reconstitution in D_2O at 20 °C, pH 7.5 on a Bruker DMX-600 spectrometer.

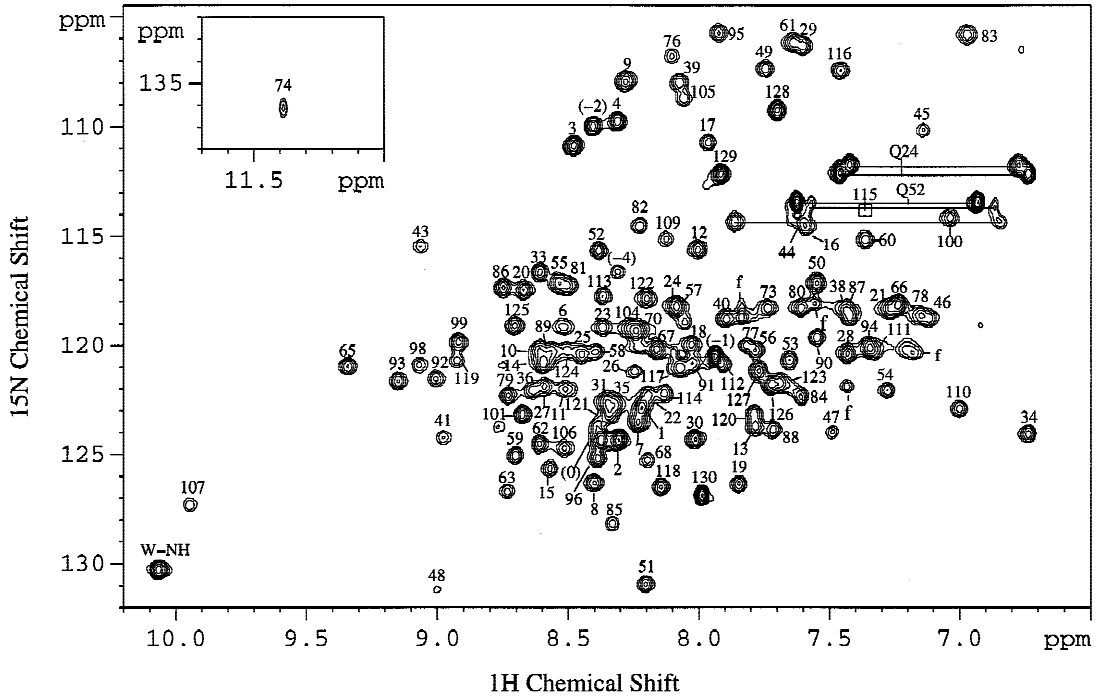

Fig. 4. ^{1}H–^{15}N HSQC spectrum of p15 protein recorded at 20 °C with backbone amides labeled. The letter "f" stands for the folded peaks. The NH resonance of Q115 is too weak to be observed at this contour level and thus is marked by a square.

mined H/D exchange rates of backbone amides at 10 °C (Yuan et al., 1999) and found most of the slowly exchanging amide protons were in the presumed helical region. These helices form four H-T-H motifs in which four conserved Gly residues (G17, G49, G83, and G116) help initiate the turns. Like the other three INK4 members, the first helix in the second H-T-H is atypical, possibly being absent or existing in a short version.

The p15 NOE assignment was an iterative process aided by p16 data and the p16 structure. Briefly, an NOE signal was tentatively assigned based on NOESY spectra comparisons with p16 (chemical shift, NOE pattern, etc.), followed by cross-checks with correlated NOEs under the local network of contact inferred from the p16 structure. Particular attention was paid to the well-separated spectral regions, such as $CH_3{}^{\delta 1}$ of an Ile residue that typically has

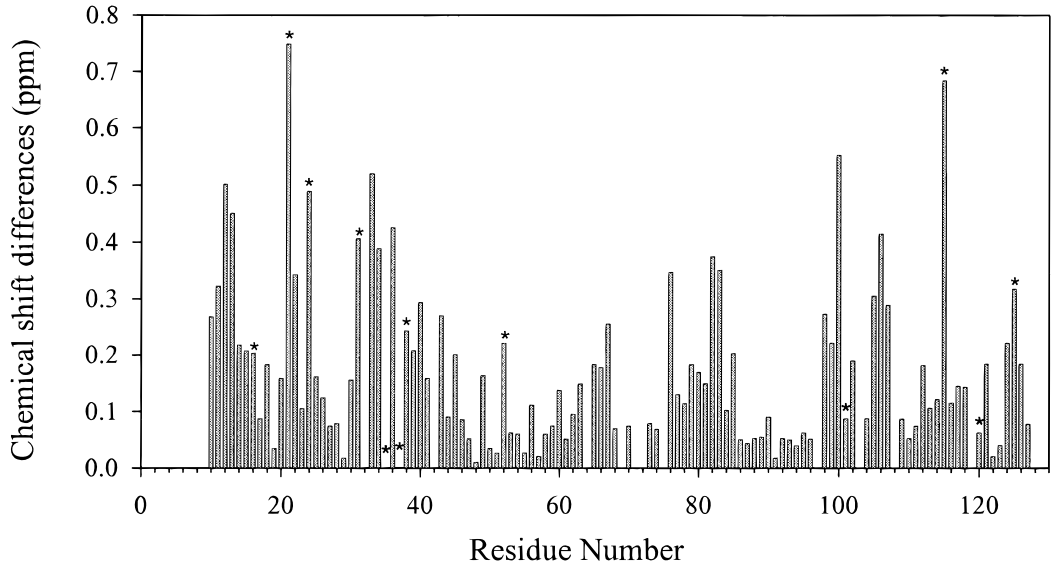

Fig. 5. Plot of combined ^{1}H and ^{15}N chemical shift differences of the two aligned p15 and p16 proteins. The differences were calculated using the equation $\Delta ppm = [(\Delta\delta_{HN})^2 + (\Delta\delta_N{*}\alpha_N)^2]^{1/2}$, in which α_N is the scaling factor (0.17) used to normalize the ^{1}H and ^{15}N chemical shifts (Farmer et al., 1996). The nonidentical residues are marked by the symbol "*."

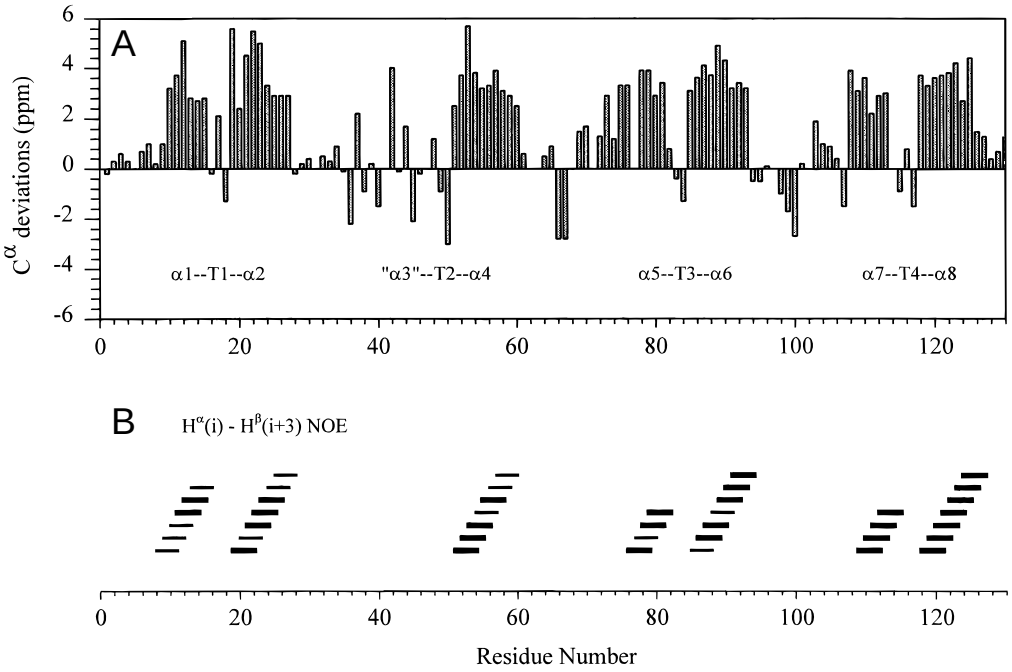

Fig. 6. Four H-T-H motifs were identified in p15. **A:** $^{13}C^{\alpha}$ chemical shift deviations from random coil values as a function of sequence numbers. **B:** Expected $H^{\alpha}(i)/H^{\beta}(i+3)$ NOEs in the helical conformations. Thick lines indicate NOEs that have been assigned. The unassigned ones are mostly due to ambiguity such as signal overlap.

an upfield ^{13}C chemical shift around 13 ppm. The overall assignments can be summarized as follows: 128 intraresidue NOEs, 259 short-range ($1 \leq i - j \leq 5$) NOEs, and 215 long-range ($5 < i - j$) NOEs. Most, if not all, of these NOE constraints are comparable to the corresponding ones in p16, strongly indicating a close similarity in the overall tertiary fold. As an example, a weak NOE between $H^{\alpha}(66)$ and $H^{\alpha}(74)$ was observed in a 2D NOESY spectrum, which is comparable to the $H^{\alpha}(73)/H^{\alpha}(80)$ NOE in $\beta 2$ of p16 (Fig. 2). This implies that p15 and p16 may have similar $\beta 2$ conformation. Figure 7 illustrates the interresidue NOE pattern observed in p15. It clearly demonstrates the close interaction between neighboring ankyrin repeats, which is in agreement with the expected feature of four H-T-H motifs linearly stacked together.

p15 structure from comparative modeling and NMR data

The MODELLER-4 program was used to generate a set of p15 structure, with the 19 final p16 structures as the templates (Šali & Blundell, 1993). The structures generated by comparative modeling have very close conformations to those of the templates. The average RMSD between p15 and p16 is <0.60 Å for the backbone heavy atoms of 8–127. On the basis of evaluation by X-PLOR, around 48 NOE violations (>0.5 Å), on average, were found among these 19 modeled structures. Violations are mostly <3 Å, and the majority of these violations are randomly distributed. The most serious violations occurred in two interresidue pairs (V19 and Q52, L35 and G39), probably as a result of the sequence difference (Q52 and L35 in p15 in contrast to R58 and P41 in p16). However, conformational differences could not be completely ruled out because, for example, L35 of p15 is located in a loop with relatively low sequence identity (R37 and F38 of p15 corresponding to S43 and Y44 in p16).

The modeled structures were then subjected to refinement with NMR data (602 NOEs and 70 H-bond constraints in the seven α-helices). The restrained energy minimization method in X-PLOR was used to minimize the NOE violations. After this process, the number of NOE violations (>0.5 Å) dropped to an average of 14, and none of the violations was >2.3 Å. More importantly, nine successful structures out of 19 were obtained from

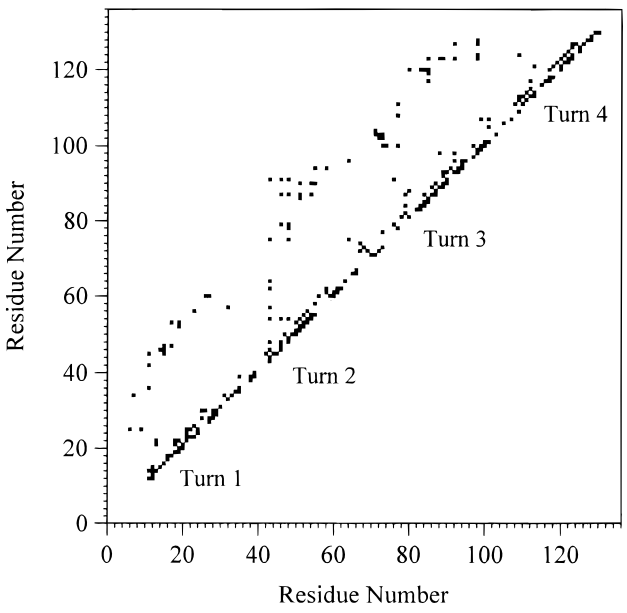

Fig. 7. Diagonal plot of the observed interresidue NOEs in p15.

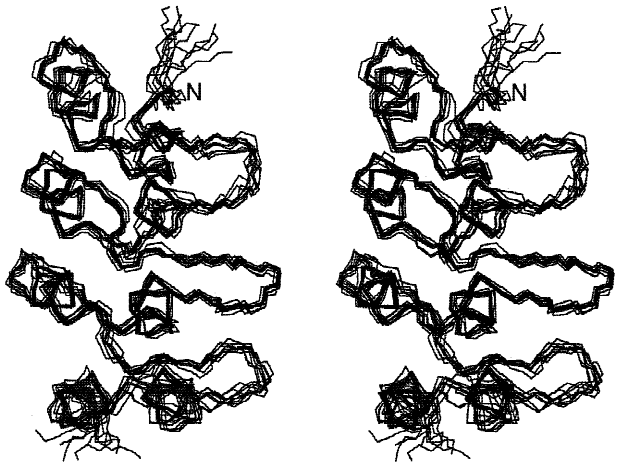

Fig. 8. Stereoview showing the best-fit superposition (average RMSD ~0.57 Å) of the backbone (N, C$^{\alpha}$, C) atoms of residues 8–127 of the 9 p15 structures. The backbone atoms of six more residues (5–7, 128–130) are also shown in this figure.

the energy minimization: they do not show NOE violations >0.5 Å. The stereochemical quality of these structures is reasonably good when analyzed by PROCHECK (Laskowski et al., 1993). For example, about 72% of the residues were located in the core of the Ramachandran plot and another 24% in the generally allowed region. Thus, the nine structures were chosen to represent the structure of the p15 protein. This ensemble is well converged (Fig. 8) and is close to the p16 conformation. It has an average backbone (N, C$^{\alpha}$, C) RMSD of 0.62 Å with respect to the mean p16 structure in the region of residues 8–127. Thus the process of restrained energy minimization can be regarded as the fine-tuning of side-chain conformations in p15.

Discussion

Structural comparisons of INK4 proteins

The p15 structural determination and the p16 structural refinement make it possible to compare the structural properties of all INK4 members, though p15 can only be called a partial NMR structure. It is obvious that INK4 proteins assume similar secondary structures and tertiary folds. For instance, the p16 and p18 NMR structures, which were determined with comparable quality now, have a backbone (N, C$^{\alpha}$, C) RMSD of 1.68 Å when p16 residues 15–134 are superimposed on p18 residues 8–127. However, they apparently have different loop conformations on the basis of the NOE assignments. First, unlike p16, p18 forms continuous β-sheets (Li et al., 1999). Second, p16 uses one more residue in making the β2 turn. These structural differences should lead to the different arrangement of side chains of binding residues (such as D74 in p16 and D67 in p18), which could contribute to the different relative affinity and/or specificity for the respective CDK. It was reported that p18, in contrast to p16, has some preference for CDK6 over CDK4 (Guan et al., 1994; Noh et al., 1999). However, different charges or polarity in the residues adjacent to conserved binding residues could also be potentially important. One such example is S43 of human p16 and the corresponding residue in all the other INK4 proteins. This residue is located on the tip of the loop 1 in all the INK4 proteins and sits between two highly conserved binding residues. Interestingly, it is Ser in p16, Gly in p18, and Arg in both p15 and p19. One may speculate that the contrasting size plus charge difference in this position could have an impact on the CDK binding. Indeed, while the side chain of Gly or Ser is far from reaching the CDK surface, the exposed, positively charged side chain of Arg in p19 was found to be in surface contact with CDK6 in both p19-CDK6 complexes (Brotherton et al., 1998; Russo et al., 1998).

Comparisons of free p16 and complexed p16

It should be noted that wild-type p16 should have L37 (Serrano et al., 1993) rather than N37, as reported in the CDK6-complexed p16 structure (Russo et al., 1998). The RMSD between the free and the complexed forms of p16 is 1.65 Å for the backbone heavy atoms of residues 14–134. Though overall they are similar, noticeable differences were found in the loop regions (Fig. 9), which could arise from either insufficient NMR data, crystal packing, or a conformational change associated with CDK6 binding. The first prominent difference is located in loop 1: RMSD is 2.9 Å for 42–46 and 3.4 Å for 44 in particular. These amino acids are involved in the interaction with CDK6: the side chain of N42 forms a hydrogen bond with the CDK6 backbone carbonyl group of V16; Y44 is in contact with C15, V16, A17, and F28 of CDK6; and R46 is in contact with Q14 of CDK6. The second prominent difference occurs in loop 2: RMSD is 2.7 Å for 74–79 and 3.9 Å for 75 in particular. In this area D74 is hydrogen bonded to R31 of CDK6. The latter also interacts with T77 and T79 of p16 through both hydrophobic and hydrogen-bonding interactions. Another important interaction appears to be the hydrophobic contact between A76 of p16 and L33 of CDK6. However, a comparatively smaller change was observed at the third loop (RMSD ~1.6 Å for 108–112). The above comparison probably can be rationalized by the X-ray result that loop 1 and loop 2 of p16 contribute more to the CDK6 binding than loop 3 does (Russo et al., 1998). It is also consistent with our observation that while site-specific substitutions of residues at loops 1 and 2 led to modest decreases in the inhibitory activity of p16 (or p18), mutations of loop 3 residues led to little change in activity (Li et al., 1999).

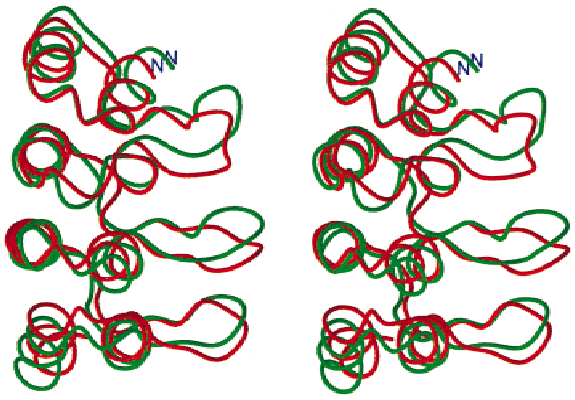

Fig. 9. Stereoview showing the ribbon drawing of best-fit superposition of the backbone (N, C$^{\alpha}$, and C) atoms of the restrained minimized mean NMR structure in a free form (red) and the X-ray structure in a complexed form (green) of p16. The coordinates of the crystal structure were obtained from the Protein Data Bank (entry 1BI7).

Comparative modeling and p15 structural determination

Comparative or homology modeling uses experimentally determined protein structures as templates to predict the conformation of other proteins with similar amino sequence (Sánchez & Šali, 1997). MODELLER is one of the most successful programs in this regard (Sánchez & Šali, 1997; Schoonman et al., 1998). It has been shown that when the target protein shares more than 40% sequence identity to the template, the results can be very accurate (Šali et al., 1995). We have many reasons to believe that the method would be successfully applied to our work: (1) All the structures of INK4 proteins (p16, p18, and p19) determined by X-ray and NMR are highly homologous, as mentioned above. (2) p15 is more than 86% sequence homologous to p16. (3) More importantly, experimental evidence from chemical shift assignments and NOE assignments strongly justifies the use of homology modeling. Unlike other modeling studies reported so far (to the best of our knowledge), we have used a significant number of experimental constraints to further refine the modeled structure. The comparative modeling method should also be well suited for structural predictions of other ankyrin-repeat proteins. As reviewed recently (Sedgwick & Smerdon, 1999), the ankyrin-repeat motif has been recognized in more than 400 proteins, such as transcriptional regulators and developmental regulators. In an ~33 residue ankyrin-repeat motif, some primary sequence consensus has been found (Sedgwick & Smerdon, 1999). Though only 14 structures (9 ankyrin-repeat proteins) by either NMR or X-ray have been reported so far, the results reveal very similar tertiary folds. Structural determination by either method is labor intensive and sometimes appears insurmountable due to instability and/or flexibility, as in the case of p15. Thus, comparative modeling will be of value to provide structural insights into a protein for functional analysis. In a broader sense, the approach used in this paper will be useful in structural genomics, because similar problems (instability of proteins and/or inability to obtain complete NMR data) could be encountered in the attempt to determine the structures of all proteins encoded by the human genome.

Materials and methods

Expression and purification of p15

The mouse p15 gene was isolated from mouse spleen total RNA by RT-PCR as described by the manufacturer (GIBCO-BRL, Gaithersburg, Maryland). First-strand DNA synthesis was performed using the following downstream primer: 5′-GCG AAT TCT CAA TCT CCA GTG GCA GCG TGC AGA TAC CTC G -3′ (with the *Eco*RI restriction site underlined). Following first-strand cDNA synthesis the DNA was amplified with the following forward primer 5′- CGG GATC CAT GTT GGG CGG CAG CAG TGA C -3′ (with the *Bam*HI site underlined) and the reverse primer as described above. The resulting DNA fragment was cut with *Bam*HI and *Eco*RI and ligated into pGEX-2T (Amersham Pharmacia Biotech, Piscataway, New Jersey). The construct was verified by DNA sequencing performed as described by the manufacturer (Perkin-Elmer, Foster City, California). The protein was expressed in a soluble form as a GST fusion protein in *Escherichia coli* BL21(DE3) cells. Isotopically labeled p15 was expressed in *E. coli* using M9 minimal medium with $(^{15}NH_4)_2SO_4$ and $^{13}C_6$-glucose as the sole nitrogen and carbon sources, respectively. The GST portion was cleaved off with thrombin and the protein was purified essentially the same as p16 (Byeon et al., 1998) and p18 (Li et al., 1999). Typical yields were 2–4 mg/L in rich media and 1–3 mg/L in minimal media. The samples were lyophilized and stored at −80 °C before use. It should be noted that the purified protein has six extra residues in the N-terminus (GSPGIH numbered from −5 to 0).

NMR experiments and assignments for structural determination of p15

All NMR experiments were performed on a Bruker DMX-600 or DRX-800 spectrometer at 20 °C. Unlabeled, uniformly ^{15}N-labeled, and uniformly ^{15}N,^{13}C-double labeled protein samples were used at concentrations of 0.2 to 0.4 mM. The samples contained 4 mM HEPES, 1 mM DTT, and 5 μM EDTA in 95% H_2O/5% D_2O or 100% D_2O at pH 7.5. The triple resonance experiments for the total assignments were conducted on the DMX-600, while all of the 2D and 3D NOESY experiments were conducted on the DRX-800 using a 100 ms mixing time. The data were processed using the XWINNMR (Bruker, Karlsruhe, Germany) or the Felix 97.0 (Molecular Simulations Inc., Burlington, Massachusetts) program. The sequence-specific resonance assignments, which were aided by the p16 results, were confirmed by $H^N(i)/H^N(i+1)$ and $H^\alpha(i)/H^N(i+1)$ NOEs from 3D ^{15}N-edited NOESY and by $^{13}C^\alpha/^{13}C^\beta$ chemical shifts from the following triple-resonance experiments: HNCA (Grzesiek & Bax, 1992a) and CBCA(CO)NH (Grzesiek & Bax, 1992b). The TOCSY experiments were not successful; thus, the chemical shift assignments as well as the NOE assignments were carried out on the 3D ^{15}N-NOESY-HSQC and 3D ^{13}C-NOESY-HMQC spectra. The ^{1}H, ^{15}N and ^{13}C assignments have been deposited in the BioMagResBank (http://www.bmrb.wis.edu) under accession number 4701.

p15 structure by comparative modeling and NMR data

The MODELLER-4 program was installed on a Silicon Graphics O2 workstation. The inputs to this program are the known structure of the template (p16) and the sequence alignment between the template and the target protein (p15). The whole sequence of mouse p15 (M1-D130) was aligned with the fragment of human p16 S7-G137 without any gap. The tertiary structure was built by invoking the "model" routine as well as reading CHARMM parameter and topology libraries. Briefly, a set of distance and dihedral angle constraints is derived from the template (p16) and transferred to the target protein (p15) based on the sequence alignment. The tertiary structure of the target protein was built by minimizing the violations of these homology-derived constraints while enforcing proper stereochemistry. Nineteen modeling structures were generated based on a set of 19 refined p16 structures. They were then subjected to 1,400 steps of restrained energy minimization (conjugate gradient algorithm) using the X-PLOR program (Brünger, 1992), with the NMR data set consisting of NOE-derived distance constraints and H-bond constraints. NOE intensities were classified into strong, medium, weak, and very weak categories. The corresponding distance constraints were specified in terms of a distance range: 1.8–2.7, 1.8–3.7, 1.8–5.0, and 1.8–6.0 Å, respectively. Hydrogen bond restraints identified in the secondary structure include $r_{NH\text{-}O}$ = 1.5–2.5 Å and $r_{N\text{-}O}$ = 2.4–3.5 Å. The quality of the final structures was externally evaluated with PROCHECK program. The structures with lowest energy and idealized geometry were selected to represent the p15 protein. The coordinates and NMR constraints have been deposited in the Protein Data Bank with accession code 1D9S.

Refinement of p16 structure

A set of 3D and 4D NOESY experiments including 3D ^{15}N-NOESY-HSQC, 3D ^{13}C-NOESY-HMQC, 4D ^{13}C-^{13}C-NOESY-HMQC, 4D ^{13}C-^{15}N-NOESY-HMQC were repeated on a Bruker DRX-800 machine using a 100 ms mixing time. The p16 structural calculations were conducted on Silicon Graphics O2 workstations or a Cray T90 Supercomputer using a simulated annealing method (Nilges et al., 1988) with the X-PLOR program. In the first stage, the simulated annealing structures were determined based on the experimental distance and dihedral angle restraints. The resulting structures were then subjected to the second stage of simulated annealing calculations where, in addition to the distance and dihedral angle restraints, the structures were refined against secondary $^{13}C^{\alpha}/^{13}C^{\beta}$ chemical shift restraints. The structures were analyzed by X-PLOR and PROCHECK, and visualized by MOLMOL (Koradi et al., 1996) and Insight II (Molecular Simulations Inc.). An ensemble of 19 converged structures was selected from a total of 60 calculations. The coordinates have been deposited in the Protein Data Bank, with accession code 1DC2 for the 19 final structures and the energy minimized mean structure.

Supplementary material in the Electronic Appendix

Two figures showing the NOE distribution as a function of p15 residue number (Supplementary Fig. 1) and the NOE violation distributions before and after energy minimization (Supplementary Fig. 2).

Acknowledgments

The authors gratefully acknowledge Dr. A. Šali for providing the MODELLER-4 software package and Alexander Showalter for critical review of the manuscript. This work was supported by NIH Grant CA 69472 to M.-D.T. and by American Cancer Society Grant IRG16-33 to I.-J.B. The study made use of a Bruker DMX-600 NMR spectrometer funded by NIH Grant RR 08299 and NSF Grant BIR-9221639, and a Bruker DRX-800 NMR spectrometer funded by the Ohio Board of Regents. Support from the Ohio Supercomputer Center is acknowledged.

References

Baumgartner R, Fernandez-Catalan C, Winoto A, Huber R, Engh RA, Holak TA. 1998. Structure of human cyclin-dependent kinase inhibitor p19^{INK4d}: Comparison to known ankyrin-repeat-containing structures and implications for the dysfunction of tumor suppressor p16^{INK4a}. *Structure 6*:1279–1290.

Brotherton DH, Dhanaraj V, Wick S, Brizuela L, Domaille PJ, Volyanik E, Xu X, Parisini E, Smith BO, Archer SJ, et al. 1998. Crystal structure of the complex of the cyclin D-dependent kinase Cdk6 bound to the cell-cycle inhibitor p19^{INK4d}. *Nature 395*:244–250.

Brünger AT. 1992. *X-PLOR: A system for X-ray crystallography and NMR*, version 3.1. New Haven, Connecticut: Yale University Press.

Byeon IJ, Li J, Ericson K, Selby TL, Tevelev A, Kim HJ, O'Maille P, Tsai MD. 1998. Tumor suppressor p16^{INK4A}: Determination of solution structure and analyses of its interaction with cyclin-dependent kinase 4. *Mol Cell 1*:421–431.

Farmer BT II, Constantine KL, Goldfarb V, Friedrichs MS, Wittekind M, Yanchunas J Jr, Robertson JG, Mueller L. 1996. Localizing the NADP+ binding site on the MurB enzyme by NMR. *Nat Struct Biol 3*:995–997.

Gemma A, Takenoshita S, Hagiwara K, Okamoto A, Spillare EA, McMemamin MG, Hussain SP, Forrester K, Zariwala M, Xiong Y, Harris CC. 1996. Molecular analysis of the cyclin-dependent kinase inhibitor genes p15$^{INK4b/MTS2}$, p16$^{INK4/MTS1}$, p18 and p19 in human cancer cell lines. *Int J Cancer 68*:605–611.

Glendening JM, Flores JF, Walker GJ, Stone S, Albino AP, Fountain JW. 1995. Homozygous loss of the p15^{INK4B} gene (and not the p16^{INK4} gene) during tumor progression in a sporadic melanoma patient. *Cancer Res 55*:5531–5535.

Grzesiek S, Bax A. 1992a. Improved 3D triple-resonance NMR techniques applied to a 31-kDa protein. *J Magn Reson 96*:432–440.

Grzesiek S, Bax A. 1992b. Correlating backbone amide and side-chain resonances in larger proteins by multiple relayed triple resonance NMR. *J Am Chem Soc 114*:6291–6293.

Guan KL, Jenkins CW, Li Y, Nichols MA, Wu X, O'Keefe CL, Matera AG, Xiong Y. 1994. Growth suppression by p18, a p16$^{INK4/MTS1}$- and p14$^{INK4B/MTS2}$-related CDK6 inhibitor, correlates with wild-type pRb function. *Genes Dev 8*:2939–2352.

Guan KL, Jenkins CW, Li Y, O'Keefe CL, Noh S, Wu X, Zariwala M, Matera AG, Xiong Y. 1996. Isolation and characterization of p19^{INK4d}, a p16-related inhibitor specific to CDK6 and CDK4. *Mol Biol Cell 7*:57–70.

Hamada K, Kohno T, Kawanishi M, Ohwada S, Yokota J. 1998. Association of CDKN2A(p16)/CDKN2B(p15) alterations and homozygous chromosome arm 9p deletions in human lung carcinoma. *Genes Chromosomes Cancer 22*:232–240.

Hannon GJ, Beach D. 1994. p15^{INK4B} is a potential effector of TGF-beta-induced cell cycle arrest. *Nature 371*:257–261.

Iolascon A, Faienza MF, Coppola B, Rosolen A, Basso G, Della Ragione F, Schettini F. 1996. Analysis of cyclin-dependent kinase inhibitor genes (CDKN2A, CDKN2B, and CDKN2C) in childhood rhabdomyosarcoma. *Genes Chromosomes Cancer 15*:217–222.

Koradi R, Billeter M, Wüthrich K. 1996. MOLMOL: A program for display and analysis of macromolecular structures. *J Mol Graphics 14*:51–55.

Laskowski RA, MacArthur MW, Moss DS, Thornton JM. 1993. PROCHECK—A program to check the stereochemical quality of protein structures. *J Appl Crystallogr 26*:283–291.

Li J, Byeon IJ, Ericson K, Poi MJ, O'Maille P, Selby T, Tsai MD. 1999. Tumor suppressor INK4: Determination of the solution structure of p18^{INK4C} and demonstration of the functional significance of loops in p18^{INK4C} and p16^{INK4A}. *Biochemistry 38*:2930–2940.

Luh FY, Archer SJ, Domaille PJ, Smith BO, Owen D, Brotherton DH, Raine AR, Xu X, Brizuela L, Brenner SL, Laue ED. 1997. Structure of the cylcin-dependent kinase inhibitor p19^{INK4d}. *Nature 389*:999–1003.

MacKie RM, Andrew N, Lanyon WG, Connor JM. 1998. CDKN2A germline mutations in U.K. patients with familial melanoma and multiple primary melanomas. *J Invest Dermatol 111*:269–272.

Malumbres M, Perez de Castro I, Santos J, Melendez B, Mangues R, Serrano M, Pellicer A, Fernandez-Piqueras J. 1997. Inactivation of the cyclin-dependent kinase inhibitor p15^{INK4b} by deletion and de novo methylation with independence of p16^{INK4a} alterations in murine primary T-cell lymphomas. *Oncogene 14*:1361–1370.

Nilges M. 1996. Structure calculation from NMR data. *Curr Opin Struct Biol 6*:617–623.

Nilges M, Clore GM, Gronenborn AM. 1988. Determination of three-dimensional structures of proteins from interproton distance data by dynamical simulated annealing from a random array of atoms. Circumventing problems associated with folding. *FEBS Lett 239*:129–136.

Noh SJ, Li Y, Xiong Y, Guan KL. 1999. Identification of functional elements of p18^{INK4C} essential for binding and inhibition of cyclin-dependent kinase (CDK) 4 and CDK6. *Cancer Res 59*:558–564.

Pinyol M, Cobo F, Bea S, Jares P, Nayach I, Fernandez PL, Montserrat E, Cardesa A, Campo E. 1998. p16(INK4a) gene inactivation by deletions, mutations, and hypermethylation is associated with transformed and aggressive variants of non-Hodgkin's lymphomas. *Blood 91*:2977–2984.

Russo AA, Tong L, Lee JO, Jeffrey PD, Pavletich NP. 1998. Structural basis for inhibition of the cyclin-dependent kinase Cdk6 by the tumour suppressor p16^{INK4a}. *Nature 395*:237–243.

Šali A, Blundell TL. 1993. Comparative protein modelling by satisfaction of spatial restraints. *J Mol Biol 234*:779–815.

Šali A, Potterton L, Yuan F, van Vlijmen H, Karplus M. 1995. Evaluation of comparative protein modeling by MODELLER. *Proteins Struct Funct Genet 23*:318–326.

Sánchez R, Šali A. 1997. Advances in comparative protein-structure modelling. *Curr Opin Struct Biol 7*:206–214.

Schoonman MJ, Knegtel RM, Grootenhuis PD. 1998. Practical evaluation of comparative modelling and threading methods. *Computers Chem 22*:369–375.

Sedgwick SG, Smerdon SJ. 1999. The ankyrin repeat: A diversity of interactions on a common structural framework. *Trends Biochem Sci 24*:311–316.

Serrano M, Hannon GJ, Beach D. 1993. A new regulatory motif in cell-cycle control causing specific inhibition of cyclinD/CDK4. *Nature 366*:704–707.

Sherr CJ. 1996. Cancer cell cycles. *Science 274*:1672–677.

Spera S, Bax A. 1991. Empirical correlation between protein backbone conformation and Cα and Cβ ^{13}C nuclear magnetic resonance chemical shifts. *J Am Chem Soc 113*:5490–5492.

Tevelev A, Byeon IJ, Selby T, Ericson K, Kim HJ, Kraynov V, Tsai MD. 1996. Tumor-suppressor p16^{INK4A}: Structural characterization of wild-type and mutant proteins by NMR and circular dichroism. *Biochemistry 35*:9475–9487.

Tsutsumi M, Tsai YC, Gonzalgo ML, Nichols PW, Jones PA. 1998. Early ac-

quisition of homozygous deletions of p16/p19 during squamous cell carcinogenesis and genetic mosaicism in bladder cancer. *Oncogene 17*:3021–3027.

Venkataramani R, Swaminathan K, Marmorstein R. 1998. Crystal structure of the CDK4/6 inhibitory protein $p18^{INK4c}$ provides insights into ankyrin-like repeat structure/function and tumor-derived $p16^{INK4}$ mutations. *Nat Struct Biol 5*:74–81.

Wüthrich K. 1986. *NMR of proteins and nucleic acids*. New York: John Wiley & Sons, Inc.

Yuan C, Li J, Selby T, Byeon IJ, Tsai MD. 1999. Tumor suppressor INK4: Comparisons of conformational properties between $p16^{INK4A}$ and $p18^{INK4C}$. *J Mol Biol 294*:201–211.

Zindy F, Soares H, Herzog KH, Morgan J, Sherr CJ, Roussel MF. 1997. Expression of INK4 inhibitors of cyclin D-dependent kinases during mouse brain development. *Cell Growth Differ 8*:1139–1150.